Research article

Journal of RAMAN SPECTROSCOPY

Received: 26 April 2012 Revised: 29 July 2012 Accepted: 13 August 2012 Published online in Wiley Online Library: 14 October 2012

(wileyonlinelibrary.com) DOI 10.1002/jrs.4184

Large-area Ag nanorod array substrates for SERS: AAO template-assisted fabrication, functionalization, and application in detection PCBs

Zhulin Huang,[a] Guowen Meng,[a,b]* Qing Huang,[c]* Bin Chen,[a] Chuhong Zhu[a] and Zhuo Zhang[a]

Highly ordered arrays of thiolated β-cyclodextrin (HS-β-CD) functionalized Ag-nanorods (Ag-NRs) with plasmonic antennae enhancement of electrical field have been achieved for encapsulation and rapid detection of polychlorinated biphenyls (PCBs). The large-area ordered arrays of rigid Ag-NRs supported on copper base were fabricated via porous anodic aluminum oxide (AAO) template-assisted electrochemical deposition. The inter-nanorod gaps between the neighboring Ag-NRs were tuned to sub-10 nm by thinning the pore-wall thickness of the AAO template using diluted H_3PO_4. The nearly perfect large-area ordered arrays of Ag-NRs supported on copper base render these systems excellent in surface-enhanced Raman scattering (SERS) performance with uniform electric field enhancement, as testified by the SERS spectra and Raman mappings of rhodamine 6 G. Furthermore, the Ag-NRs were functionalized with HS-β-CD molecules so as to capture the apolar PCB molecules in the hydrophobic cavity of the CD. Compared to the ordinary undecorated SERS substrates, the HS-β-CD modified Ag-NR arrays exhibit better capture ability and higher sensitivity in rapid detection of PCBs. Copyright © 2012 John Wiley & Sons, Ltd.

Supporting information may be found in the online version of this article.

Keywords: surface-enhanced Raman scattering; anodic aluminum oxide; Ag nanorod array; β-cyclodextrin; polychlorinated biphenyls

Introduction

Polychlorinated biphenyls (PCBs) belong to a class of persistent organic pollutants that threaten the ecosystem and cause significant toxicity to human beings.[1] PCBs can bio-accumulate in fatty tissues through food chains, so even small exposures may eventually reach dangerous levels (2.7 to 20.5 mg/kg in killer whale).[2] To date, the PCBs can still be found in high concentrations in soils, waste disposal sites, natural waters, and in the aquatic life of these waters.[3,4] Traditional techniques for the detection of PCBs mainly include high-resolution capillary gas chromatographic,[5] immunoassays,[6] and high-resolution mass spectrometry.[7] However, these methods are generally expensive and time-consuming. Therefore, rapid and sensitive detection of PCBs is important.

Surface-enhanced Raman scattering (SERS) spectroscopy is a powerful tool for real-time ultrasensitive detection of chemicals of trace amount,[8–11] or even at the single-molecule level,[12–15] by providing the specific structural and vibrational fingerprints of the interested analytes. Controlling the plasmonic 'hot spots' over a large area of a SERS substrate for sensitive and reproducible Raman response has been a major focus in the development of robust and practical SERS probes to trace chemicals such as environmental pollutants.[16–18] However, general SERS substrates based on Ag and Au, either in the form of dispersed nanoparticles or ordered nanoparticle, nanowire, and nanorod arrays,[19–23] are difficult to release reliable SERS effect for facing two challenges: first, it is required to have a large-area SERS substrate with regularly arranged nanostructures containing well-controlled narrow gaps (normally < 10 nm) that can induce the hot spots; second, even if the nanostructures have the regular arrays of hot spots, it is also required to capture the interested molecules effectively and homogenously on the surface of the SERS substrate.[24] While people have strived to deal with the first challenge by fabricating well-ordered arrays of silver dimer and bowtie nanoantenna using the advanced lithographic techniques,[25,26] the second one may be equally important but ignored to some extent, and it is actually not so easy to tackle. For example, to detect PCBs using SERS, it is found that PCBs do not readily anchor to the locations where the hot spots reside on a normal noble metal SERS substrate.[27,28]

* *Correspondence to: Guowen Meng, Key Laboratory of Materials Physics and Anhui Key Laboratory of Nanomaterials and Nanostructures, Institute of Solid State Physics, Chinese Academy of Sciences, P. O. Box 1129, Hefei 230031, P. R. China. E-mail: gwmeng@issp.ac.cn*

* *Qing Huang, Key Laboratory of Ion Beam Bioengineering, Hefei Institutes of Physical Science, Chinese Academy of Sciences, Hefei 230031, P. R. China. E-mail: huangq@ipp.ac.cn*

a *Key Laboratory of Materials Physics and Anhui Key Laboratory of Nanomaterials and Nanostructures, Institute of Solid State Physics, Chinese Academy of Sciences, P. O. Box 1129, Hefei 230031, P. R. China*

b *University of Science and Technology of China, Hefei 230026, P. R. China*

c *Key Laboratory of Ion Beam Bioengineering, Hefei Institutes of Physical Science, Chinese Academy of Sciences, Hefei 230031, P. R. China*

Journal of RAMAN SPECTROSCOPY

Cyclodextrins (CDs) belong to homochiral cyclic oligosaccharides consist of six or more α-D-glycopyranose units forming a sort of truncated cone with a polar outside and an apolar cavity. Due to the hydrophilic hydroxyl groups outside, CDs can be dissolved in water, and due to the hydrophobic property of the apolar cavity, CDs can encapsulate a variety of poorly water-soluble organic compounds.[29,30] Recent theoretical predictions show that β-CD can efficiently include the guest PCB molecule with 1:1, 2:1, and 2:2 stoichiometries.[31]

Herein, for the SERS-based detection of PCBs, we demonstrate that the two problems can be solved by a combinational procedure of fabricating large-area patterned arrays of robust sub-10-nm gapped Ag-nanorods (Ag-NRs) via electrochemical deposition (ECD) using porous anodic alumina oxide (AAO) template and subsequently modifying the exposed Ag-NRs with thiolated β-CD (HS-β-CD). On one hand, by using a copper substrate as supporter, the large-area arrays of aligned Ag-NRs with sub-10-nm gaps can provide uniform surface morphology for reproducible SERS signals. On the other hand, the HS-β-CD molecules can connect to the Ag-NR through the readily formed Ag–S bond between the functional group –SH of HS-β-CD and the Ag-NR surface,[32] and capture PCB molecules which match the size of the hydrophobic cavities of HS-β-CD. As expected, the resultant arrays of HS-β-CD functionalized Ag-NRs with high density of 10-nm gaps have trapped PCB molecules effectively and homogenously on the hot spots of the substrate, generating strong and reproducible SERS signals.

Experimental

Materials

Oxalic acid, silver nitrate, ethylene diamine tetraacetic acid (EDTA), potassium phosphate dibasic, sodium sulfite, orthophosphoric acid, copper sulfate pentahydrate, boric acid, and sodium hydroxide were purchased from Sinopharm Chemical Reagent limited corporation. Rhodamine 6 G (R6G) and *para*-aminothiophenol (*p*-ATP) were obtained from Sigma Aldrich. HS-β-CD was customized from Shandong Binzhou Zhiyuan Bio-Technology Co., Ltd. PCB77, PCB29, and PCB101 were purchased from AccuStandard. Milli-Q deionized water (resistivity = 18.2 MΩcm^{-1}) was used for all preparations.

Fabrication of Ag-NR arrays

The arrays of Ag-NRs were fabricated by using AAO template-assisted ECD approach.[33] First, the through-pore AAO templates were prepared via a two-step anodization of pure aluminum foil in oxalic acid (0.3 M) aqueous solution under 40 V_{DC} at 10 °C for at least 14 h. The barrier layer was removed, and the pores were widened subsequently via wet chemical etching in diluted H_3PO_4 (5%) aqueous solution at 40 °C for 30–50 min. A silver layer (50–100 nm) was sputtered onto one planar surface side of the through-pore AAO template to serve as working electrode. Then, Ag-NRs were pulsed electrodeposited inside the template channels at a shifted potential of 0.4–0.8 V at 15 °C, using an electrolyte containing $AgNO_3$ (10 g L^{-1}), EDTA (5 g L^{-1}), Na_2SO_3 (50 g L^{-1}), and K_2HPO_4 (20 g L^{-1}). Upon a typical pulsed ECD duration of 1–5 min, a strong copper base was electrodeposited onto the bottom surface of the AAO template embedded with Ag-NR arrays, using an electrolyte containing $CuSO_4 \cdot 5H_2O$ (160 g^{-1}) and H_3PO_4 (30 g^{-1}). Finally, the AAO template was completely removed by immersing in 5% H_3PO_4 to expose the arrays of Ag-NRs that supported on the copper base.

SERS measurements

Prior to exposures to any analyte (R6G and PCBs), the Ag-NR arrays were cleaned in argon plasma for 5 min to remove the

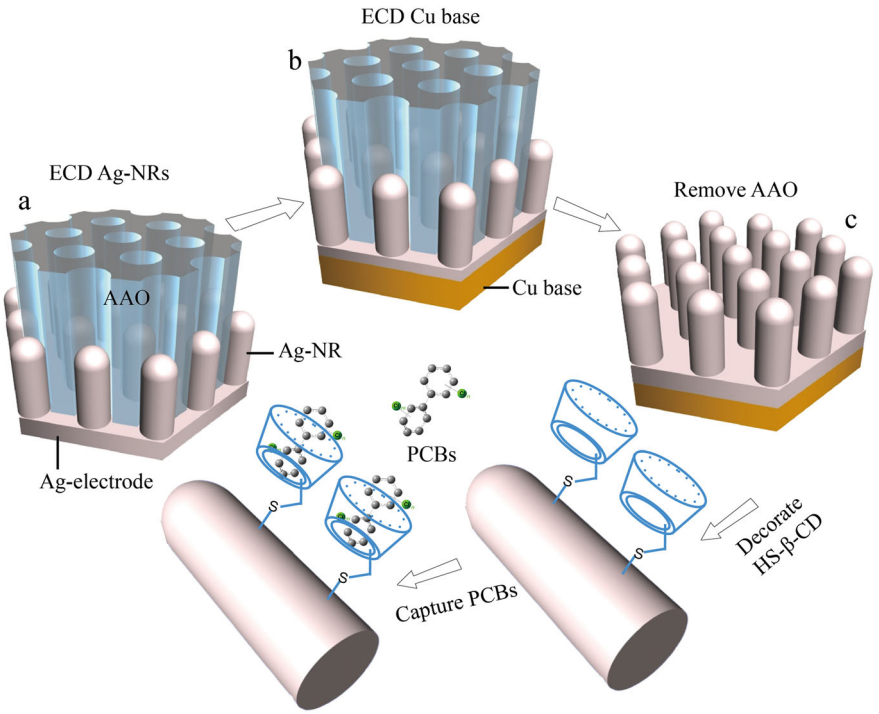

Figure 1. Schematic showing the fabrication of Cu-base-supported arrays of HS-β-CD decorated Ag-NRs for effective capturing PCB molecules in SERS detection.

surface contamination. For test of SERS sensitivity, 10-μL R6G solutions at varied concentrations were dispersed on the substrates using a micro-pipettor and dried at ambient environment to remove any surface moisture. For the SERS detection of PCBs (PCB77, PCB101, PCB29), PCBs were dissolved in acetone and diluted to varied concentrations. Pieces of the HS-β-CD modified SERS substrates, i.e. copper base-supported arrays of Ag-NRs decorated with a layer of HS-β-CD molecules, were dipped in varied concentrations of PCB acetone solutions for 4 h, dried, and tested. All the SERS spectra were measured by a confocal microprobe Raman spectrometer (Renishaw, Invia) with a 532 nm laser line, where the effective power of the laser source was 0.03 mW for R6G molecules, and 0.3 mW for PCB molecules. The laser spot focused on the sample surface was about 10 μm in diameter. Raman mappings of R6G were collected by using the Renishaw StreamLine accessory with a step size of 2 μm at 532 nm laser line.

Theoretical simulation

Finite-element method modeling

Finite-element method (FEM) modeling was conducted by using the RF module of Comsol Multiphysics V3.5a, parameters were based on those of the Ag-NR arrays from scanning electron microscopy (SEM) observations, such as the central distance between all the adjacent NRs (100 nm), the diameters of the NRs (45–95 nm), the length of the NRs (~200 nm), together with the excitation line of 532 nm. Optical constants of Ag were acquired from the literature.[34]

Calculation of the Raman spectra of PCBs

The vibrational assignments of PCB molecules were calculated by using Gaussian 03 W software at B3LYP/6-31 G(d) level.

Results and discussion

Procedure of fabrication of HS-β-CD decorated Ag-NR arrays

The fabrication scheme is shown in Fig. 1. Instead of using as-anodized routine AAO template with larger pore-wall thickness (40 nm) between the adjacent pores in our previous work,[35] here, we used pore-widened AAO template with sub-10-nm pore-wall thickness as template. A segment of Ag-NRs (shown in Fig. 1a) was electrodeposited into the bottom section of the pore-widened AAO template with Ag film coated on the bottom surface side electrode.[36] Then, a thick layer of copper base (shown in Fig. 1b) was electrodeposited onto the bottom Ag electrode of the Ag-NRs embedded AAO template to 'support' and 'strengthen' the Ag-NRs instead of using organic resin layer.[35] After wet chemical etching the AAO template (shown in Fig. 1c), the resultant

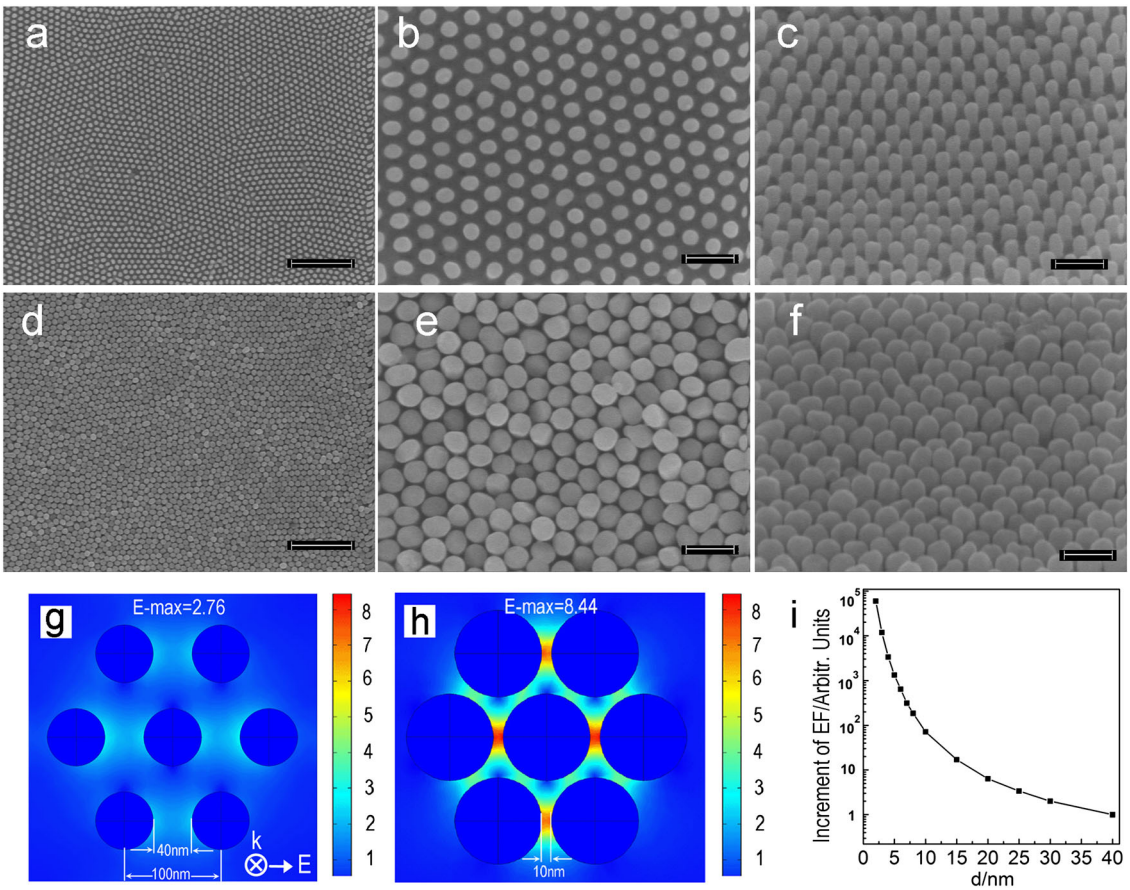

Figure 2. a) SEM image of large-area Ag-NR arrays with 40-nm gap, b) close-up view of the Ag-NR arrays, and c) the corresponding oblique view of the 40-nm-gap Ag-NR arrays. d) SEM image of large-area Ag-NR arrays with 10-nm gap, e) close-up view of the Ag-NR arrays, and f) the corresponding oblique view of the 10-nm-gap Ag-NR arrays showing uniform 10-nm gaps. Scale bars are 1 μm for Fig. 2a and Fig. 2d, 200 nm for all the other SEM images. g) and h) E-field intensity distributions (indicated by the color bar) of the Ag-NR arrays with 40-nm gaps and 10-nm gaps, the aspect ratio is 3 and 2.3, respectively. i) The increment of EF along with the reduction of inter-nanorod gaps by FEM simulations.

Journal of RAMAN SPECTROSCOPY

fully exposed, highly ordered, and well-aligned robust Ag-NRs were stably and strongly fixed on the supporting Cu layer, ensuring the handy manipulation and reliable SERS measurement of organic chemicals. Subsequently, the Ag-NRs were exposed to HS-β-CD aqueous solution (0.1 mg/ml) for 2 h and rinsed in deionized water, so that the HS-β-CD molecules can immobilize on the surface of the exposed Ag-NRs through Ag–S bond and capture target PCB molecules,[31,32] by taking advantage of the size-selective molecular encapsulation and the hydrophobic cavity of the β-CD.[37]

Characterization of the Ag-NR arrays

By utilizing pore-widened AAO template with varied pore-wall thicknesses, arrays of Ag-NRs with gaps between the adjacent NRs ranging from 40 nm to 10 nm were readily fabricated. With an H_3PO_4 (5%) etching duration 30 min at 40 °C, the pore-wall thickness of AAO template can be tuned to 40 nm. Figure 2a shows the top view of Ag-NR arrays with 40-nm inter-nanorod gaps at a large area, attributing to the excellent supporting effect of the copper layer. Figure 2b is the close-up view of vertically aligned arrays of Ag-NRs. Figure 2c is the corresponding oblique view, showing high density uniform 40-nm gaps between the adjacent Ag-NRs. With an H_3PO_4 (5%) etching duration 50 min at 40 °C, the pore-wall thickness of AAO template was readily adjusted to sub-10 nm, as demonstrated by the SEM images of Ag-NR arrays with 10-nm gaps (Fig. 2d, e, and f). Besides, the nanorod length can also be adjusted by simply controlling the ECD durations. Upon an ECD duration 2 min, the Ag-NR about 200 nm has been achieved, as demonstrated by a typical transmission electron microscope image of Ag-NR arrays with 10-nm gaps, and an aspect ratio around 2.3, which can sufficiently promote the longitudinal mode excitation of the surface plasmon of the Ag-NRs (Fig. S1, Supporting Information).[38]

FEM modeling of Ag-NR arrays

To elucidate the gap-induced localized plasmon coupling between the adjacent Ag-NRs for highly active SERS effect, we used FEM modeling to investigate the localized electric field intensity of the arrays of Ag-NRs with varied gaps.[39,40] The electric field intensity profiles are plotted, as shown in Fig. 2g and 2h, where the corresponding inter-nanorod gap is 40 nm and 10 nm, respectively. The maximum value of the electric field intensity (E-max) in the presented cross sections is 2.76 V/m and 8.44 V/m, respectively, suggesting that the large electromagnetic enhancement of the Ag-NR arrays stems from the 10-nm gaps between the adjacent NRs. Considering the fourth power dependence of enhancement factor (EF) on the electric field intensity,[41] the EF would increase by two orders with the abridgement of inter-NR gaps from 40 nm to 10 nm (Fig. 2i). Obviously, the diameter of the Ag-NRs would change due to the confined central distance between adjacent Ag-NRs (100 nm) and the varied pore-wall thickness. Again, FEM modeling was used to probe the localized E-field enhancement for Ag-NRs with varied diameter but the same length and gap. Generally, the field enhancement will get slightly weaker in a certain diameter range of the Ag-NRs with increasing of the nanorod diameter (Fig. S2, Supporting Information).

Actual sensitivity of the Ag-NR arrays

To verify the improved SERS performance of the Ag-NR arrays with 10-nm gaps between the neighboring NRs, we compared

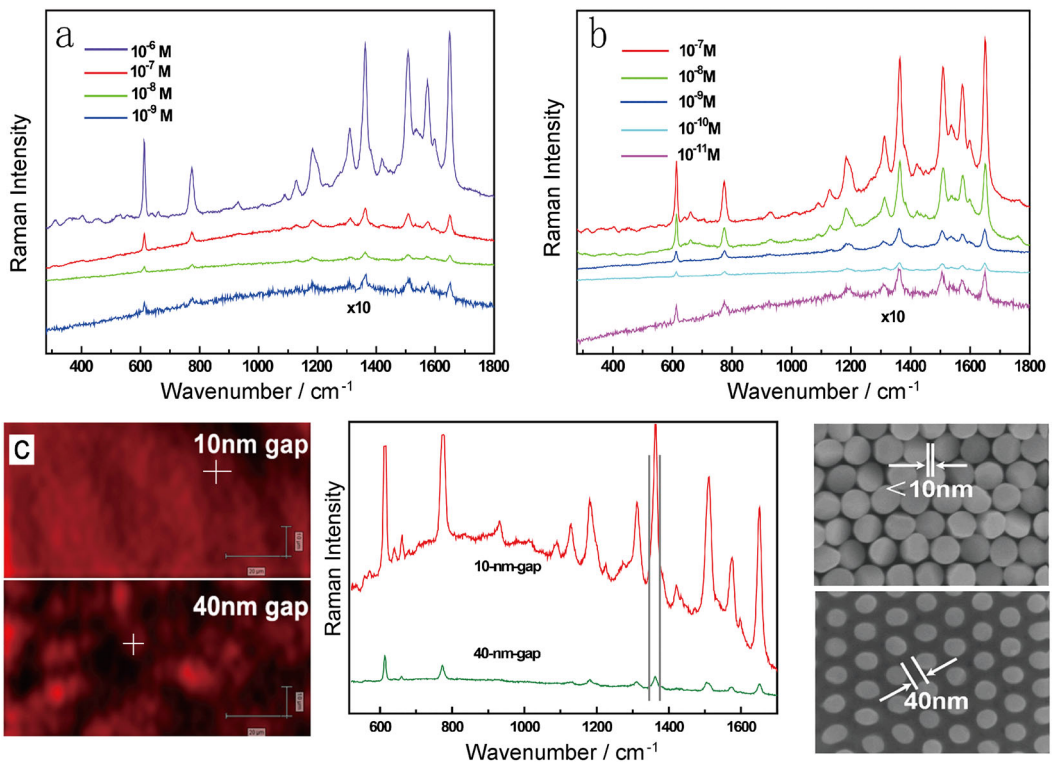

Figure 3. SERS spectra of R6G with varied concentrations dispersed on the arrays of Ag-NRs with a) 40-nm gaps and b) 10-nm gaps. c) Left: Raman mappings ($100 \times 50\ \mu m^2$, step = 2 μm, 918 spectra) of the 1361 cm^{-1} shift of 10^{-7} M R6G probe molecules adsorbed on the arrays of Ag-NRs with 40-nm gaps (lower mapping) and 10-nm gaps (upper mapping); Middle: SERS spectra at two random spots taken from the corresponding arrays of Ag-NRs as indicated by the crosses inside; Right: SEM images of the corresponding arrays of Ag-NRs with 10-nm gaps and 40-nm gaps.

two typical Ag-NRs substrates, where the gap distance is 40 nm achieved via as-anodized routine AAO template (NR length ~ 180 nm, aspect ratio ~ 3) and 10-nm gap (NR length ~ 210 nm, aspect ratio ~ 2.3). By maintaining the same measurement conditions, using R6G aqueous solutions with varied concentrations as the probe molecule, the SERS spectra in Fig. 3a demonstrate high quality SERS signals at high R6G concentrations (10^{-6}–10^{-8} M), and low signal/noise ratio spectra at 10^{-9} M concentration for the arrays of Ag-NRs with 40-nm gap. Nevertheless, very intense characteristic Raman bands at the same 10^{-9} M concentration emerge from the Ag-NR arrays with 10-nm gaps (Fig. 3b). Even when the R6G solution is further diluted to 10^{-11} M, the characteristic bands of R6G are still clearly visible. Further Raman mappings (Fig. 3c) demonstrate that the 10-nm-gap Ag-NR arrays exhibit excellent surface uniformity and larger field enhancement than those of the 40-nm-gap Ag-NR arrays due to the electric field intensity differences in their plasmonic coupling between the adjacent Ag-NRs.

To estimate the EF of SERS substrates, the formula $EF = (I_{SERS}/N_{SERS})/(I_{RS}/N_{RS})$ is applied,[42] where I_{SERS} and I_{RS} represent the relative band intensities of the SERS spectra and the Raman spectra (non-SERS), respectively, and N_{SERS} and N_{RS} represent the number of molecules on the substrates within the laser spot. The average EF is estimated to be 1.6×10^5 for the SERS substrate with 40-nm gap between the adjacent NRs with an aspect ration of 3, and 3×10^7 for the arrays of 10-nm-gap NRs with an aspect ration of 2.3 (Supporting Information Part S2). Thus, the abridgement of gap distance has increased the EF value by two orders of magnitude, being in coincidence with our previous FEM theoretical simulation results.

Signal reproducibility of the Ag-NR arrays

Conceivably, the robustness of the copper base-supported Ag-NR arrays has well ensured the substrate uniformity in SERS measurements. By measuring several random spots across the whole Ag-NR arrays, using two probe molecules of 10^{-8} M R6G and 10^{-6} M *p*-ATP as analytes respectively, the maximum intensity derivation with respect to the average intensity is calculated to be 18% for the 614 cm^{-1} band of R6G (10^{-8} M) and 8% for the 1143 cm^{-1} band of *p*-ATP (10^{-6} M), respectively, indicating that the SERS spectra can be reproducible to a great extent (Fig. S4, Supporting Information).

SERS detection of PCBs

Due to the apolar nature, PCBs can hardly be dissolved in water or adsorbed to the Ag-NR surface. Without the adsorption of PCB molecules, we can not reach higher detection sensitivity. To capture more PCB molecules, it is essential to modify the HS-β-CD onto the Ag-NRs. For this purpose, the commercially obtained HS-β-CD molecules were connected to the Ag-NR surface through the Ag–S bond, as verified by the X-ray photon-electron spectroscopy (Fig. 4). As indicated in Fig. 5a, the optimized dimensions of PCB77 range from 0.52 nm to 1.02 nm, suggesting that the hydrophobic cavity of β-CD with diameters ranging from 0.557 nm of the bottom rim to 0.747 nm of the upper rim are capable of encapsulating some PCB molecules and forming 1:1 host (CD)–guest (PCB) complex at a thermodynamically stable state.[31]

To evaluate the trapping validity of the HS-β-CD functionalized Ag-NR arrays toward PCBs, PCB77 – one congener of PCBs – was used, and the SERS Raman spectra are shown in Fig. 5b. We

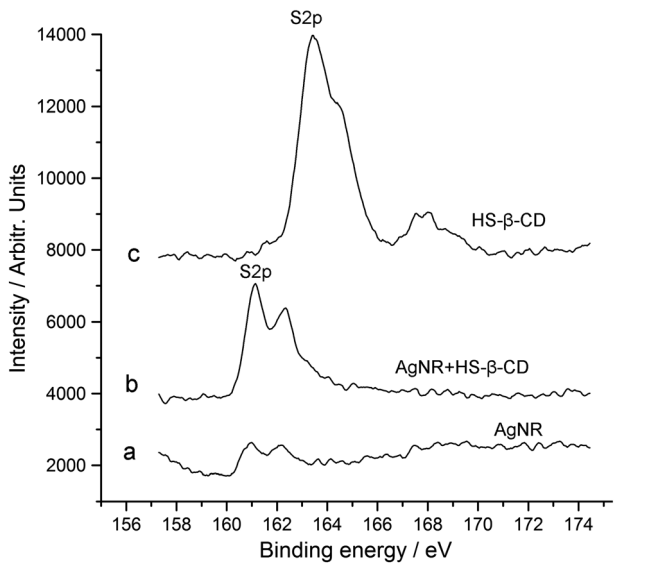

Figure 4. Selected XPS spectra (X-ray photoelectron spectroscopy, Thermo ESCALAB 250) from Ag-NRs before (curve a) and after (curve b) the exposure to HS-β-CD molecules, the slight shift of binding energy of S2p qualitatively indicate the successful decoration of HS-β-CD onto Ag-NRs. Curve c) is the XPS spectrum of HS-β-CD for comparison. The intensities of the spectra have been shifted for clarity.

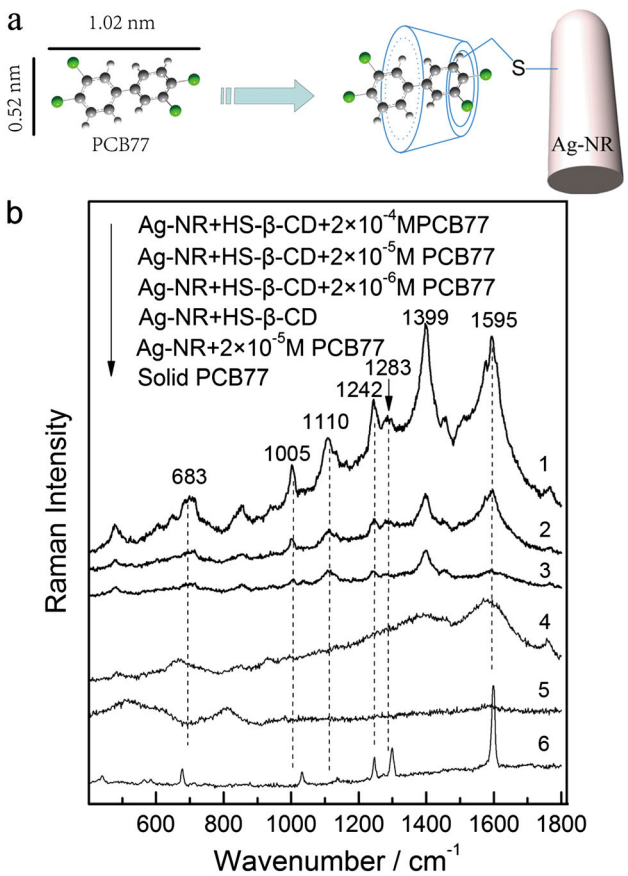

Figure 5. a) Scheme showing the encapsulation of PCB77 molecule by HS-β-CD decorated Ag-NR, the PCB77 geometric dimensions are derived by using the optimized structure from the B3LYP/6-31 G(d) calculations. b) SERS spectra of PCB77 by using the HS-β-CD functionalized Ag-NR arrays (shown in Fig. 2d) as SERS substrates.

Journal of RAMAN SPECTROSCOPY

Table 1. Major observed and calculated fingerprint Raman vibrational assignments of PCB77, PCB29, and PCB101

Molecule	Vibrational description	Observed/cm^{-1}		Calculated [a]
		Powder	SERS	
PCB 77	Ring stretching	1596	1598	1580
	C–C bridge stretching	1300	1283	1271
	C–H wagging	1248	1242	1230
	C–Cl stretching	1136	1110	1115
	Trigonal breathing	1032	1005	1004
	C–Cl stretching	679	683	690
PCB 29	Aromatic ring stretching	1604/1584	1584	1598/1565
	C–H wagging	1502	1494	1488
	Ring breathing	1347	1338	1324
	C–C bridge stretching	1266	1246	1240
	Ring trigonal breathing	1004	1004	999/1018
	C–Cl stretching	710	710	685
PCB 101	Aromatic ring stretching	1601	1598	1583
	C–H wagging	1387	1390	1396
	Ring trigonal breathing	1284	1277	1288
	C–C bridge stretching	1241	1240	1245
	C–Cl stretching	1145	1139	1128
	Trigonal breathing	1035	1032	1032
	C–Cl stretching	697	689	675

[a]Calculated at B3LYP/6-31 G(d) level, the vibrational wavenumbers are scaled by an optimal factor 0.9613.

analyze the SERS spectra and the normal Raman spectrum of PCB77 (Fig. 5b, curve 6) by using Gaussian 03w software at B3LYP/6-31 G(d) level (Table 1).[43,44] In comparison with the normal Raman spectrum of solid PCB77, the characteristic peaks (Fig. 5b, curve 1, 2, and 3) at positions of 683 cm^{-1}, 1005 cm^{-1}, 1110 cm^{-1}, 1242 cm^{-1}, 1283 cm^{-1}, and 1595 cm^{-1} are recognized as the vibrational fingerprint bands of PCB77 captured by HS-β-CD functionalized Ag-NR arrays, except the peak at 1399 cm^{-1} that is attributed to disordered carbon formed on the SERS substrate.[45] The strong vibrational mode at 1595 cm^{-1} can be assigned to aromatic ring stretching mode. For comparison, we also measured the SERS spectra of PCB77 using the bare Ag-NR arrays (without the decoration of HS-β-CD) as SERS substrate, but no pronounced characteristic peaks can be identified (Fig. 5b, curve 5), demonstrating the poor affinity of the bare Ag-NRs toward PCB molecules and the effective capture of PCB77 after the Ag-NRs being functionalized with HS-β-CD molecules.

To further demonstrate the capturing ability of the CD 'pockets', we tested other PCB congeners — PCB29 and PCB101. The SERS spectra in Fig. 6a and Fig. 6b show the well-resolved peaks at 2×10^{-5} M for PCB29 and PCB101 using the HS-β-CD functionalized Ag-NRs arrays as SERS substrates. Without the decoration of HS-β-CD, no apparent vibrational fingerprints of PCBs can be observed even at a high concentration of 2×10^{-4} M. Although the detection concentration of PCBs is not satisfied, the HS-β-CD functionalized Ag-NRs do show improvement in detection trace PCB77, PCB101, and PCB29.

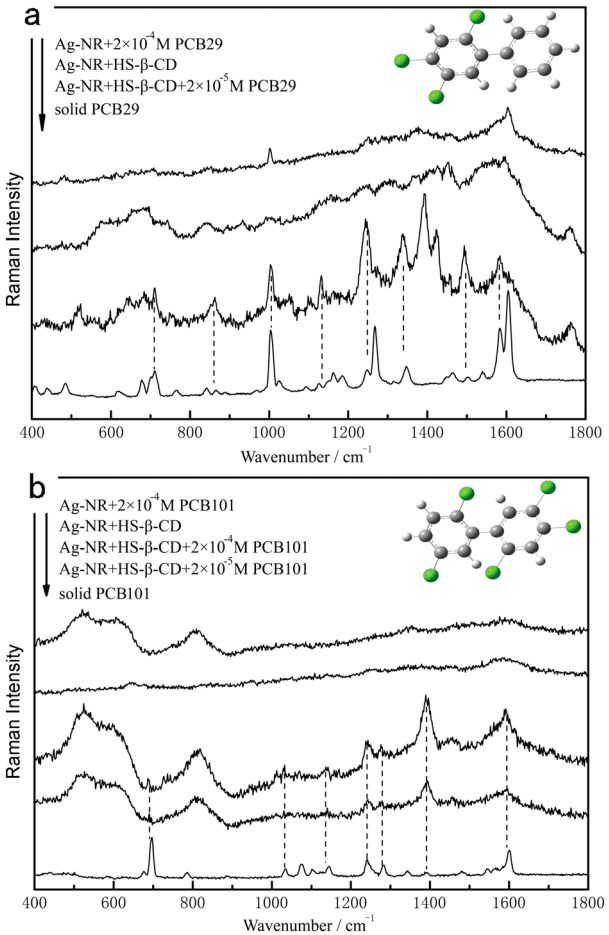

Figure 6. a) SERS spectra of PCB29 measured from the HS-β-CD decorated (two middle curves) and undecorated (upper curve) Ag-NR arrays. The lower curve is the Raman spectrum of solid PCB29 for comparison. b) SERS spectra of PCB101 measured from the HS-β-CD decorated (two middle curves) and undecorated (upper curve) Ag-NR arrays. The lower curve is the Raman spectrum of solid PCB101 for comparison.

Conclusions

In summary, we have designed and achieved large-scale arrays of highly ordered and vertically aligned robust Ag-NRs as SERS substrate, which can provide a huge number of uniformly distributed sub-10-nm gaps between the adjacent Ag-NRs. By chemically modifying the Ag-NRs with a monolayer of HS-β-CD molecules that contain hydrophobic cavity matching the size of PCB molecules, congeners of PCBs can be effectively captured, and so the SERS detection capability can be further improved. This concept of highly ordered arrays of the HS-β-CD functionalized Ag-NRs supported on copper base may open a new door to design robust, reproducible, sensitive SERS substrates for rapid and reliable detection of trace organic pollutants in the environment.

Acknowledgements

We thank the National Key Basic Research Program of China (Grant 2013CB934304), the National Natural Science Foundation of China (Grants 51201159, 11274312, 50972145, and 11175204), and the Key Innovative Project of Chinese Academy of Science (Grant KJCX2YWN341) for the financial support.

Supporting information

Supporting information may be found in the online version of this article.

References

[1] P. G. Shields, *Cancer Epidemiol. Biomarkers Prev.* **2006**, *15*, 830.
[2] M. Noël, L. Barrett-Lennard, C. Guinet, N. Dangerfield, P. S. Ross, *Mar. Environ. Res.* **2009**, *68*, 196.
[3] D. L. Lewis, A. W. Garrison, K. E. Wommack, A. Whittemore, P. Steudler, J. Melillo, *Nature* **1999**, *401*, 898.
[4] G. G. Ying, C. A. Rawson, R. S. Kookana, M. S. Warne, P. A. Peng, X. M. Li, E. Laginestra, L. A. Tremblay, J. C. Chapmanf, R. P. Lim, *J. Environ. Monit.* **2009**, *11*, 1687.
[5] M. D. Mullin, C. M. Pochini, S. McCrindle, M. Romkes, S. H. Safe, L. M. Safe, *Environ. Sci. Technol.* **1984**, *18*, 468.
[6] USEPA. Method 4020, OSW, Ed. 2003. www.epa.gov/osw/hazard/testmethods/sw846/pdfs/4020.pdf
[7] USEPA. Method 1668B, 2008. www.epa.gov/waterscience/methods/method/files/1668.pdf
[8] M. Mulvihill, A. Tao, K. Benjauthrit, J. Arnold, P. D. Yang, *Angew. Chem. Int. Ed.* **2008**, *47*, 6456.
[9] K. Carron, L. Peltersen, M. Lewis, *Environ. Sci. Technol.* **1992**, *26*, 1950.
[10] S. R. Dasary, A. K. Singh, D. Senapati, H. Yu, P. C. Ray, *J. Am. Chem. Soc.* **2009**, *131*, 13806.
[11] G. Braun, S.-J. Lee, M. Dante, T. Nguyen, M. Moskovits, N. Reich, *J. Am. Chem. Soc.* **2007**, *129*, 6378.
[12] S. Nie, S. Emory, *Science* **1997**, *275*, 1102.
[13] K. Kneipp, Y. Wang, H. Kneipp, L. Perelman, I. Itzkan, R. Dasari, M. Feld, *Phys. Rev. Lett.* **1997**, *78*, 1667.
[14] J. Camden, J. Dieringer, Y. Wang, D. Masiello, L. Marks, G. Schatz, R. P. Van Duyne, *J. Am. Chem. Soc.* **2009**, *78*, 12616.
[15] S. M. Stranahan, K. A. Willets, *Nano Lett.* **2010**, *10*, 3777.
[16] M. Moskovits, *J. Raman Spectrosc.* **2005**, *36*, 485.
[17] C. L. Jones, K. C. Bantz, C. L. Haynes, *Anal. Bioanal. Chem.* **2009**, *394*, 303.
[18] S. Abalde-Cela, S. Ho, B. Rodríguez-González, M. A. Correa-Duarte, R. A. Álvarez-Puebla, L. M. Liz-Marzán, N. A. Kotov, *Angew. Chem. Int. Ed.* **2009**, *48*, 5326.
[19] J. Theiss, P. Pavaskar, P. M. Echternach, R. E. Muller, S. B. Cronin, *Nano Lett.* **2010**, *10*, 2749.
[20] M. Hu, F.-S. Ou, W. Wu, I. Naumov, X. M. Li, A. M. Bratkovsky, R. S. Williams, Z. Y. Li, *J. Am. Chem. Soc.* **2010**, *132*, 12820.
[21] C. M. Ruan, G. Eres, W. Wang, Z. Y. Zhang, B. H. Gu, *Langmuir* **2007**, *33*, 5757.
[22] H.-H. Wang, C.-Y. Liu, S.-B. Wu, N.-W. Liu, C.-Y. Peng, T.-H. Chan, C.-F. Hsu, J.-K. Wang, Y.-L. Wang, *Adv. Mater.* **2006**, *18*, 491.
[23] S.-J. Lee, A. R. Morrill, M. Moskovits, *J. Am. Chem. Soc.* **2006**, *128*, 2200.
[24] P. Aldeanueva-Potel, E. Faoucher, R. A. Alvarez-Puebla, L. M. Liz-Marzán, M. Brust, *Anal. Chem.* **2009**, *81*, 9233.
[25] Y. Sawai, B. Takimoto, H. Nabika, K. Murakoshi, *J. Am. Chem. Soc.* **2007**, *129*, 1658.
[26] A. Hatab, C.-H. Hseuh, A. L. Gaddis, C. T. Retterer, J.-H. Li, G. Eres, Z. Y. Zhang, B. H. Gu, *Nano Lett.* **2010**, *10*, 4952.
[27] L. Guerrini, J. V. Garcia-Romos, C. Domingo, S. Sanchez-Cortes, *Anal. Chem.* **2009**, *81*, 953.
[28] K. E. Shafer-Peltier, C. L. Haynes, M. R. Glucksberg, R. P. Van Duyne, *J. Am. Chem. Soc.* **2003**, *125*, 588.
[29] T. Thorsteinn Lofsson, M. E. Brewster, *J. Pharm. Sci.* **1996**, *85*, 1017.
[30] J. Szejtli, *Pure Appl. Chem.* **2004**, *76*, 1825.
[31] P. Liu, D. J. Zhang, J. H. Zhan, *J. Phys. Chem. A* **2010**, *114*, 13122.
[32] J. Wang, L. Kong, Z. Guo, J. Xu, J. Liu, *J. Mater. Chem.* **2010**, *20*, 5271.
[33] D. C. Yang, G. W. Meng, C. H. Zhu, X. G. Zhu, *Chem. Commun.* **2009**, 7110.
[34] M. A. Ordal, L. L. Long, R. J. Bell, S. E. Bell, R. R. Bell, R. W. Alexander, Jr., C. A. Ward, *Appl. Opt.* **1983**, *22*, 1099.
[35] Z. L. Huang, G. W. Meng, Q. Huang, Y. J. Yang, C. H. Zhu, C. L. Tang, *Adv. Mater.* **2010**, *22*, 4136.
[36] C. H. Zhu, G. W. Meng, Q. Huang, Z. B. Li, Z. L. Huang, M. L. Wang, J. P. Yuan, *J. Mater. Chem.* **2012**, *22*, 2271.
[37] J. Liu, J. Alvarez, A. E. Kaifer, *Adv. Mater.* **2000**, *12*, 1381.
[38] G.-H. Gu, J. Kim, L. Kim, J.-S. Suh, *J. Phys. Chem. C* **2007**, *111*, 7906.
[39] M. Micic, N. Klymyshyn, Y.-G. Suh, H. Peter Lu, *J. Phys. Chem. B* **2003**, *107*, 1574.
[40] N. Calander, M. Willander, *J. Appl. Phys.* **2002**, *92*, 4878.
[41] F. J. García-Vidal, J. B. Pendry, *Phys. Rev. Lett.* **1996**, *77*, 1163.
[42] E. C. Le Ru, E. Blackie, M. Meyer, P. G. Etchegoin, *J. Phys. Chem. C* **2007**, *111*, 13794.
[43] H. A. Jiménez-Vázquez, J. Tamariz, R. James Cross, *J. Phys. Chem. A* **2001**, *105*, 1315.
[44] S. K. Ignatov, P. G. Sennikov, A. G. Razuvaev, L. A. Chuprov, O. Schrems, B. S. Ault, *J. Phys. Chem. A* **2003**, *107*, 8705.
[45] Y. J. Yang, G. W. Meng, *J. Appl. Phys.* **2010**, *107*, 044315.